Supplementary Information (SI) for Physical Chemistry Chemical Physics.

Supplementary information

Mechanisms of CO_2 and H_2O Co-adsorption Behavior on Functionalized Porous Carbons: Perspectives of Molecular Clustering Effect

Hongyu Chen[a], Da Wei[a], Wenji Pi[a], Peixin Wang[a], Kueasook Ratchadaporn[a], Yong Liu[a], Peng He[a], Zijie Sun[b], Changqing Su[c], Xiang Xu[a, *], Zheng Zeng[a, *] and Liqing Li[a, *]

[a] *School of Energy Science and Engineering, Central South University, Changsha 410083, China*

[b] *Beijing Spacecrafts, China Academy of Space Technology, Beijing, 100094, China*

[c] *Hunan Key Laboratory of Carbon Neutrality and Intelligent Energy, School of Resources & Environment, Hunan University of Technology and Business, Changsha 410205, China*

* Corresponding author.

E-mail address: xuxiang@csu.edu.cn (Xiang Xu)

E-mail address: zengzheng@csu.edu.cn (Zheng Zeng)

E-mail address: liqingli@hotmail.com (Liqing Li)

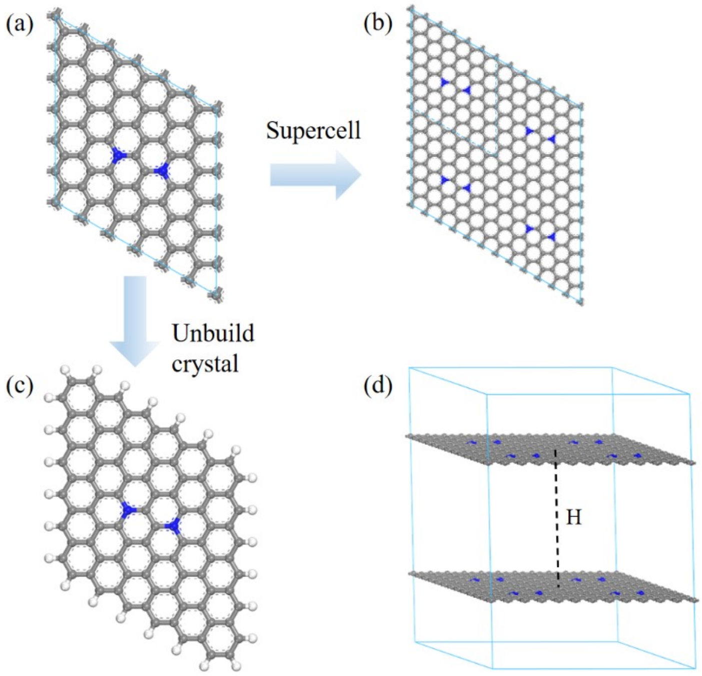

Fig. S1 Optimized structures of (a) unit cell, (b) supercell and (c) aperiodic models. (c) Schematic diagram of molecular model with pore size H. Gray and blue atoms represent carbon and nitrogen atoms, respectively.

The graphite slit pore model in this work adopts the AB stacking (Bernal stacking) mode, which is the most stable crystal structure of natural graphite, and is consistent with the stacking mode of graphitized regions in real porous carbon materials. In the GCMC and MD simulations, the position and stacking mode of the graphene sheets are fixed, and only the gas molecules in the pore space are allowed to move, which is the conventional setting for gas adsorption simulations in carbon slit pores.

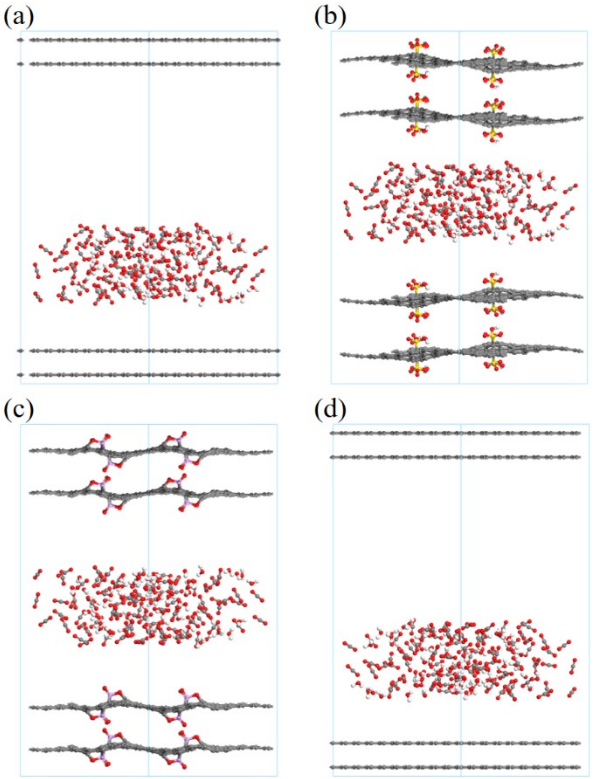

Fig. S2 Atomistic representation of CO_2 and H_2O adsorbed on the multi-layer graphite layer structure formed by G-None and G-Rs.

Graphite is a three-dimensional crystal formed by stacking the multiple layers of graphene through van der Waals forces. Graphene is a two-dimensional material composed of a single layer of carbon atoms arranged in a hexagonal honeycomb pattern. It is known from the experiments or high-precision quantum chemical calculations that the carbon-carbon bond length in graphite is approximately 1.42 Å. Hence, it can be calculated that the unit cell of graphene is a rhombus with a side length of $a = b \approx 2.46$ Å and an angle of 120°. To simulate the larger-sized graphene sheets or study the defects, adsorption, etc., we need to repeat the original cells in a plane to construct supercells. The graphene constructed by the supercell has periodic boundary conditions in both the x and y directions in the plane, simulating an infinitely large graphene sheet. Then, add a sufficiently thick vacuum layer in the direction perpendicular to the plane (z direction) to ensure that there is no false interaction between the mirror images of the upper and lower layers of graphene.

By constructing a multi-layer graphite layer model that is completely parallel and extends to infinity in all directions, the real carbon and pore morphology of porous carbon can be more accurately represented.[1,2] In the molecular dynamics simulation of this study, the graphene model was staggered and stacked, with 2 layers stacked up and down and 4 layers in total (Fig. S2). The second layer performs a translation relative to the first layer in the plane. The atoms of the second layer are placed above the center of the six-membered ring on first layer. Thus, half of the atoms of the second layer are exactly above the atoms of the first layer, and the other half are directly above the center of the six-membered ring on first layer. However, these stacking models were not taken into account in the subsequent DFT calculations. One reason is the non-periodic model adopted in the DFT calculations, and the other is that during the structural optimization process, the upper graphene sheet has little deformation relative to the lower graphene sheet. Adding a large number of atoms will exponentially increase the DFT calculation time. Therefore, to ensure the rationality and practicality of the calculation, the DFT calculation is optimized on one layer of carbon sheet and the subsequent first-principles calculations are carried out.

Table S1 Atomic partial charges (e) for surface functional groups (Rs) and their adjacent C atoms (C_d) on G-Rs and G-None.

Rs	None	NH_2	$C{=}O$	SO_3H	C_3—P	(CO)C_2PO
H	–	0.301~0.301	–	0.284~0.284	–	–
C	0.178~0.178	–	-0.704~-0.704	–	-0.438~-0.342	-1.573~-0.983
N	–	-0.539~-0.539	–	–	–	–
O	–	–	-0.128~-0.128	-0.107~0.144	–	0.090~0.109
S	–	–	–	-0.047~-0.047	–	–
P	–	–	–	–	0.991~1.024	0.446~0.446
C_d	0.059~0.059	-0.172~-0.172	-0.141~-0.141	-0.251~-0.251	0.017~0.087	-1.266~0.600

Table S2 Lennard-Jones parameters of functionalized and pristine graphene models.

	H	C	N	O	P	S
σ (Å)	2.85	3.47	3.26	3.03	3.70	3.59
ε (K)	0.05	47.85	38.95	48.16	161.02	173.10

Table S3 Lennard-Jones parameters and atomic partial charges of gas molecules.

	σ (Å)	ε (K)	q (e)
C (CO_2)	2.80	27.00	0.700
O (CO_2)	3.05	79.00	-0.350
H (H_2O)	0.00	0.00	0.336
O (H_2O)	2.67	135.00	-0.672

Grand canonical Monte Carlo simulation is one of the gold standard computational methods for studying the adsorption behavior of porous materials. However, the validity of its conclusion strongly depends on a fundamental assumption: the adsorption process is mainly driven by the physical interactions. When there is significant chemical adsorption within the system, the standard GCMC simulation becomes inaccurate. GCMC simulation relies on a pre-parameterized force field to describe the interactions between atoms and molecules. These force fields are adept at capturing the physical adsorption interactions, such as van der Waals forces, electrostatic interactions, polar interactions, and weak π-π stacking. Chemical adsorption involves the formation and breaking of chemical bonds between molecules and surfaces, which is usually accompanied by the redistribution of electrons and significant charge transfer. This process falls within the realm of quantum mechanics. The standard and classic GCMC force field is non-reactive, meaning that chemical bonds cannot form or break during the simulation process. Possible chemical reactions between CO_2 and amino groups, such as carbamate, carbamic acid, or bicarbonate formation, are not included in the present GCMC model. The –NH_2 group considered in this work should be regarded as a representative nitrogen-containing surface functionality on porous carbon, rather than as a model of amine-grafted solid sorbents dominated by CO_2 chemisorption.

Therefore, the validity of GCMC simulation is based on the assumption that the adsorption process is mainly dominated by the non-bonding interactions. When there is significant chemical adsorption in the system, this fundamental assumption is broken, leading to the distorted simulation results. Thus, a limitation of the present work is that CO_2–amine chemisorption was not considered. Such reactions could be important for amine-rich adsorbents, especially under humid conditions. Future studies will require reaction-informed or reactive simulation methods to couple physical adsorption, water clustering, and CO_2–amine chemistry in a unified model.

(a) None

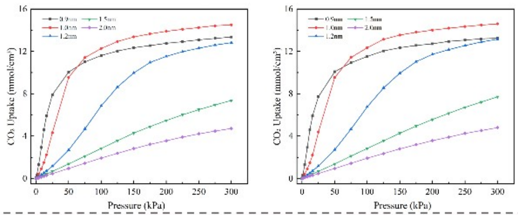

(b) NH_2

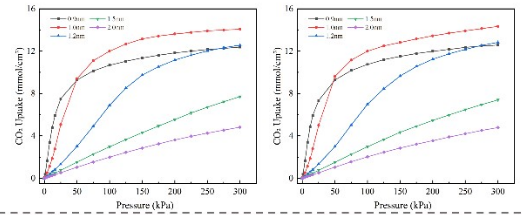

(c) Pyridinic-N

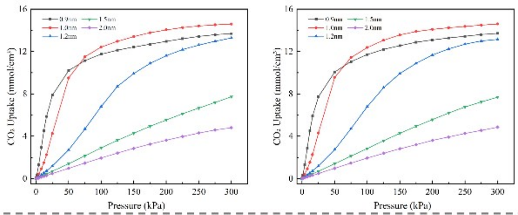

(d) Graphitic-N

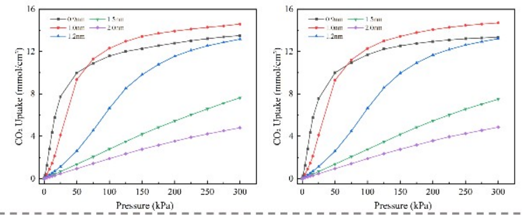

(e) COOH

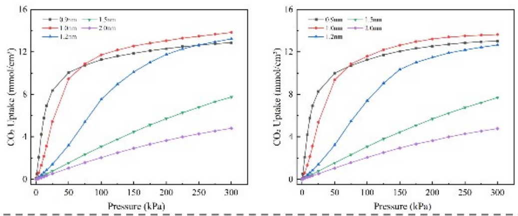

(f) OH

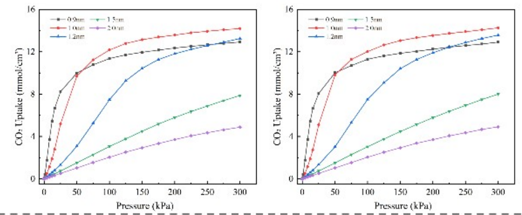

(g) C=O

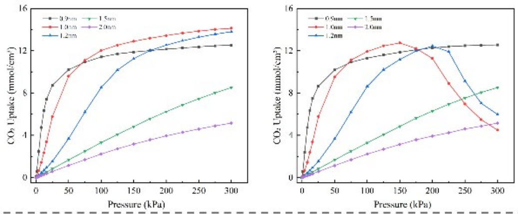

(h) SO

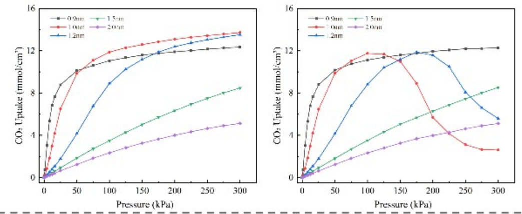

(i) SO_2

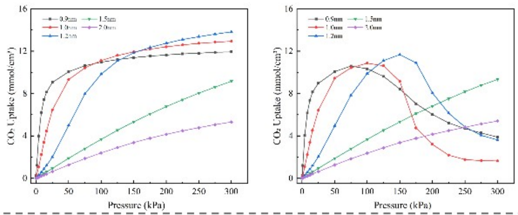

(j) SO_3H

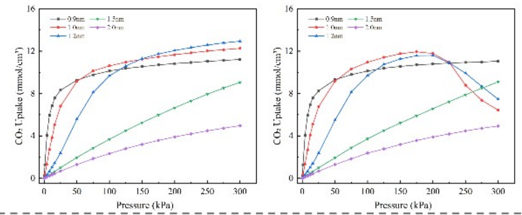

(k) C_3-P

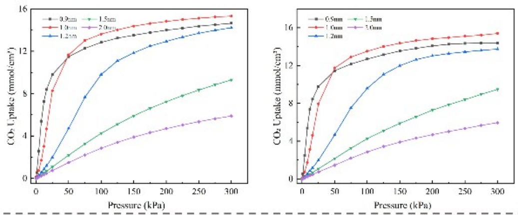

(l) C_3-P=O

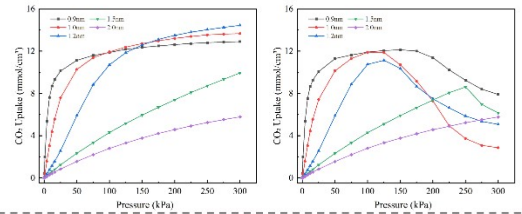

(m) $(CO)C_2PO$

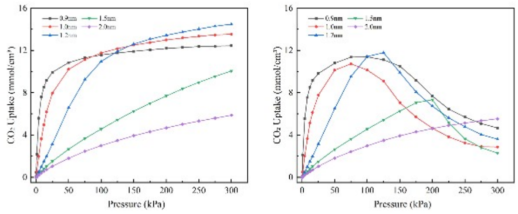

(n) $CO-PO(OH)_2$

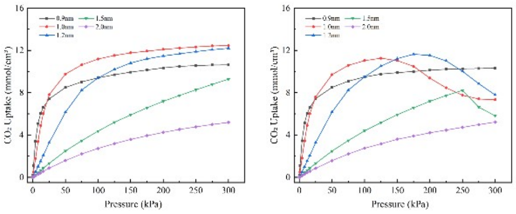

Fig. S3 Absolute adsorption isotherms of CO_2 on (a) G-None and (b-n) G-Rs with different pore sizes (0.9-2.0 nm) at 298 K and dry (left) and humidity (right) conditions.

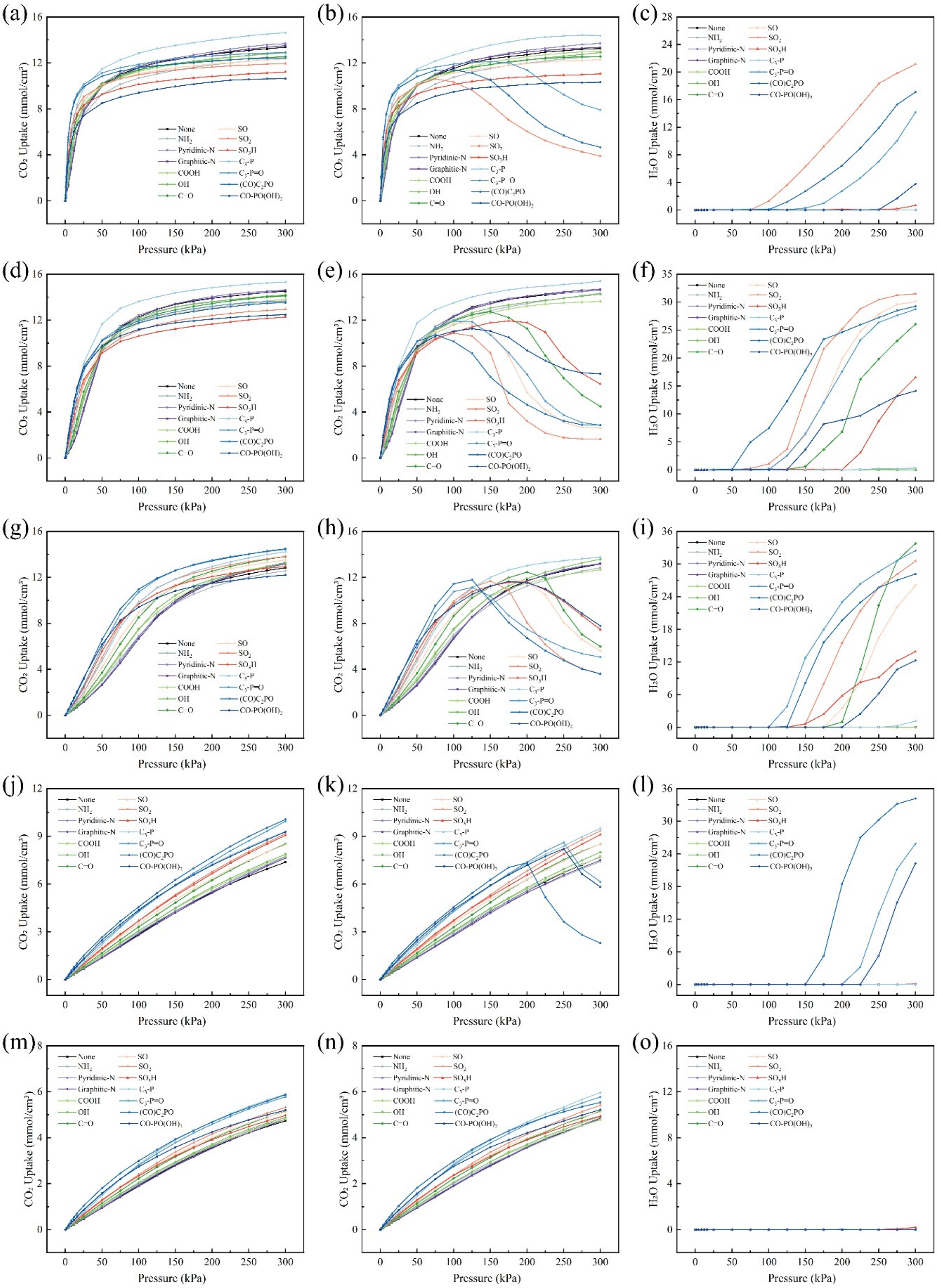

Fig. S4 Absolute adsorption isotherms of CO_2 (left and middle) and H_2O (right) on G-None and G-Rs with a pore size of 0.9 nm (a-c), 1.0 nm (d-f), 1.2 nm (g-j), 1.5 nm (j-l), and 2.0 nm (m-o) under dry (left) and humidity conditions (middle and right).

Understanding weak intermolecular interactions, including van der Waals force, hydrogen bonding, electrostatic interaction, and π-effects, is foundational to advance molecular design in chemistry, materials science, and biology. Since Yang et al. reported the visual analysis method of weak interactions (non-covalent interaction (NCI)), which graphically show the areas, types and strengths of weak interactions in a chemical system [3], visual analysis of weak interactions has been widely used and become one of the standard methods for studying weak interactions. After this, many researchers switched to the more intuitive and physically meaningful visual analysis methods of weak interactions, such as density overlap regions indicator (DORI) [4], independent gradient model (IGM) [5], interaction region indicator (IRI) [6] and independent gradient model based on Hirshfeld partition (IGMH) [7]. Different methods have their own characteristics, nature and main occurrence region. Among them, the IGMH method has attracted increasing attention since it can intuitively visualize all kinds of interactions between defined fragments with accurate color reflecting and less computation time.

In IGMH analysis, the intermolecular interaction region is visualized by three-dimensional function δg. Meanwhile, $sign(\lambda_2)\rho$ is mapped on the isosurfaces by different colors to visually characterize the nature of intermolecular interactions. $sign(\lambda_2)\rho$ represents the product of electron density ρ and sign of second largest eigenvalue of Hessian matrix of ρ. ρ in interaction region is generally positively correlated with the interaction strength, while $sign(\lambda_2)$ has certain ability to distinguish between attractive and repulsive interactions. The coloring method and description of $sign(\lambda_2)\rho$ in different value ranges is given in Fig. S5.

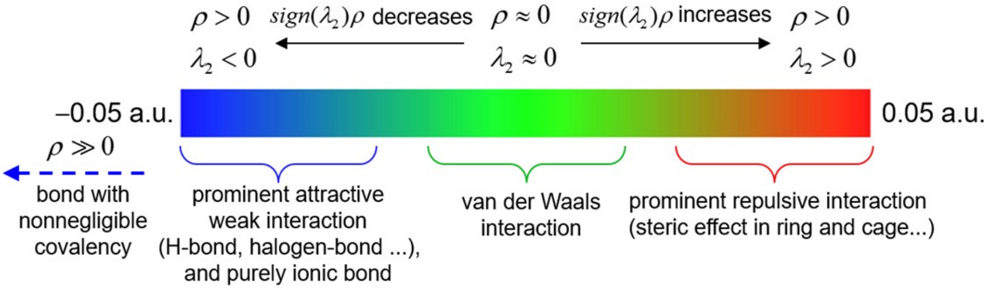

Fig. S5 Color scale and corresponding interpretation for mapping function $sign(\lambda_2)\rho$ on IGMH isosurfaces.

As shown in Fig. S5, the color scale of $sign(\lambda_2)\rho$ for van der Waals interaction show green on isosurface, because the region of van der Waals interaction always has a relatively low electron density ($\rho \approx 0$). Furthermore, the regions corresponding to prominent attractive weak interaction (H-bond and halogen-bond) or obvious repulsive interaction (steric effects in ring and cage) exhibit a larger electron density ($\rho > 0$), and the corresponding color scale is blue and red, respectively.

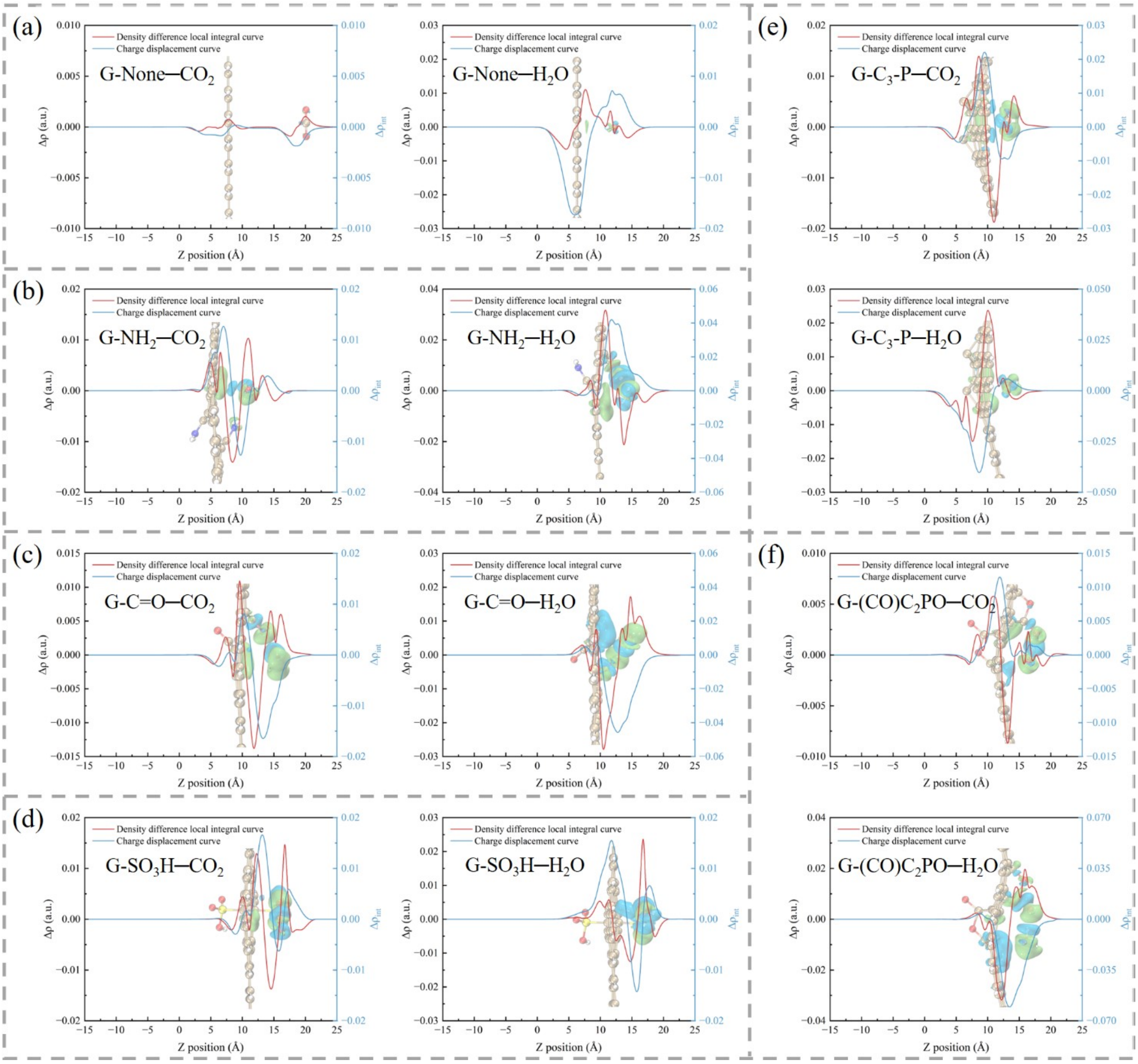

Fig. S6 Electron density difference between gas molecule and adsorption surface and the corresponding electron density local integral curve and charge displacement curve. The green and blue isosurfaces show the increase and decrease of electron density after adsorption, respectively, and the isosurface value is set as 3×10^{-4} e/Å^3.

Electron density difference (EDD) is a popular method for analyzing bonding and electron transfer.[8] The weak interaction between fragments is often accompanied by a change in electron, and a significant increase or decrease in electron density on the bonding region reflects the weakening or strengthening of corresponding interaction.[9] According to the isosurface maps in Fig. S6, it is observed that the regions between gas molecule and G-Rs gather a high density of gained/donated electrons, which is the key representation of bonding. For example, after CO_2 molecule is combined with G-(CO)C_2PO configuration, the electron density on C and O atoms of CO_2 is drastically reduced, which is transferred to the direction of -(CO)C_2PO group to a large extent. While G-None─CO_2 shows a relatively weak electron redistribution. Beyond that, the electron density local integral curve and charge displacement curve quantitatively discuss and compare the net gaining and donating of electrons and charge transfer quantity at different cross sections. It can be found that the electron density increases significantly in the area where CO_2 molecule is bonded with G-(CO)C_2PO due to the intermolecular interaction, and there is an obvious positive value of 0.012 e at 11.74 Å on charge displacement curve, which indicates a net transfer of 0.012 electron from CO_2 to G-(CO)C_2PO. The other adsorption configurations of G-Rs exhibit the similar electron density difference and charge transfer, especially for G-Rs─H_2O adsorption configurations (except G-C_3─P), showing a stronger charge redistribution and higher charge transfer than that for CO_2, which is consistent with the results of E_{ads}.

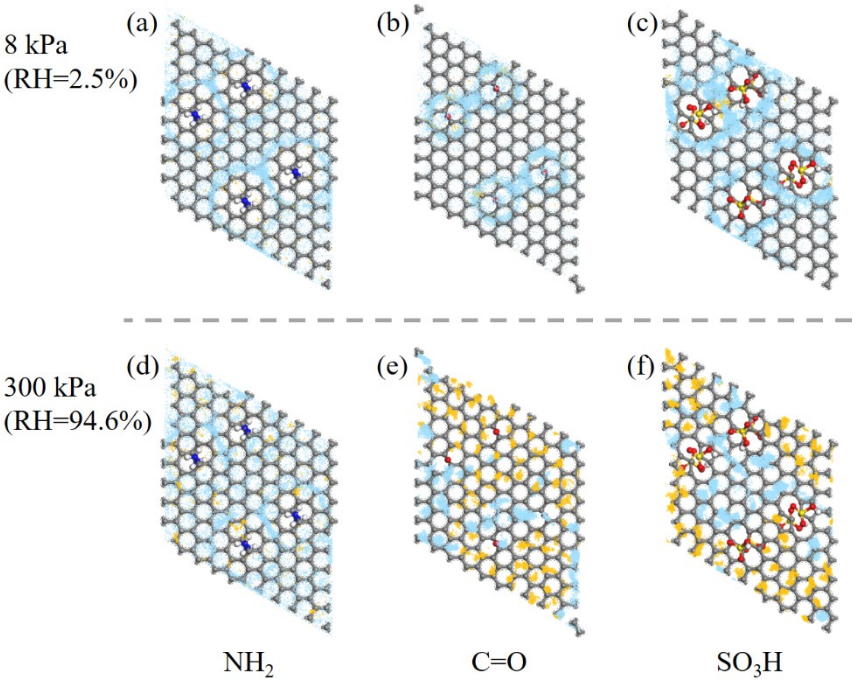

Fig. S7 Density distribution maps of CO_2 and H_2O on G-NH_2, G-C═O and G-SO_3H at 8 kPa (RH=2.5%) and 300 kPa (RH=94.6%). Blue points represent the adsorption density of CO_2, and orange points represent the adsorption density of H_2O.

References

1 L. F. Salas-Guerrero, S. Builes and G. A. Orozco, *Int. J. Hydrogen Energy*, 2024, **50**, 1626-1633.

2 K. T. Thomson and K. E. Gubbins, *Langmuir*, 2000, **16**, 5761-5773.

3 E. R. Johnson, S. Keinan, P. Mori-Sánchez, J. Contreras-García, A. J. Cohen and W. Yang, *J. Am. Chem. Soc.*, 2010, **132**, 6498-6506.

4 P. de Silva and C. Corminboeuf, *J. Chem. Theory Comput.*, 2014, **10**, 3745-3756.

5 C. Lefebvre, G. Rubez, H. Khartabil, J.-C. Boisson, J. Contreras-García and E. Hénon, *Phys. Chem. Chem. Phys.*, 2017, **19**, 17928-17936.

6 T. Lu and Q. Chen, *Chemistry–Methods*, 2021, **1**, 231-239.

7 T. Lu and Q. Chen, *J. Comput. Chem.*, 2022, **43**, 539-555.

8 W. Zhang, J. Yin, P. Zhang, X. Tang and Y. Ding, *J. Mater. Chem. A*, 2018, **6**, 12029-12037.

9 X. Li, L. Zhu, X. Chang, D. He, Q. Xue and W. Xing, *J. Mater. Chem. A*, 2018, **6**, 12404-12410.